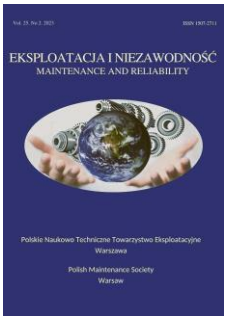

Eksploatacja i Niezawodnosc – Maintenance and Reliability
Volume 28 (2026), Issue 4
journal homepage: http://www.ein.org.pl

Article citation info:
Sun Y, Sun Y, Huang Y, Yu J, Zhou X, Dynamic resilience assessment of combat system of systems: A dual-dimensional framework integrating mission and inherent capabilities, Eksploatacja i Niezawodnosc – Maintenance and Reliability 2026: 28(4) http://doi.org/10.17531/ein/219911

Dynamic resilience assessment of combat system of systems: A dual-dimensional framework integrating mission and inherent capabilities

Indexed by: Web of Science Group

Yusheng Sun[a], Yuxiang Sun[b], Yijie Huang[c], Jiahui Yu[a], Xianzhong Zhou[a,*]

[a] School of Management and Engineering, Nanjing University, China
[b] School of Robotics and Automation, Nanjing University, China
[c] North Automatic Control Technology Institute, China

Highlights

- Combat System of Systems resilience is evaluated through a dual-dimensional framework incorporating standby units.
- Dynamic resilience is characterized from the perspectives of mission capability and inherent capability.
- Long-term confrontation scenarios are addressed with a multi-phase dynamic resilience evaluation method.
- Simulation experiments and wargame case studies demonstrate the importance of standby units and the applicability of the model.

Abstract

In dynamic confrontation scenarios, units within combat system of systems (CSoS) exhibit dual states: mission-active and standby. Standby units, serving as critical reserves for sustained combat operations, significantly influence system resilience continuity. Existing dynamic resilience research primarily assesses system capability through mission-active units' performance, neglecting the quantification of standby units' contributions to resilience evolution. To bridge this gap, this study proposes a dual-dimensional resilience assessment framework that integrates real-time mission performance metrics with the inherent reconnaissance and strike capabilities of standby units. This approach simultaneously quantifies instantaneous combat capability and latent recovery potential. Additionally, addressing the sensitivity degradation in resilience assessment due to cumulative disruption effects in prolonged confrontations, we design a dynamic phase-segmented resilience evaluation model (DPS-RE) that incorporates dynamic, time-varying performance baselines. Simulation experiments verify the regulatory influence of standby units on CSoS degradation and validate the effectiveness of targeted resource replenishment strategies. Furthermore, utilizing multi-domain joint combat simulation data, the DPS-RE model effectively identifies vulnerability windows and provides early warnings for resource supplementation, offering robust decision support in dynamic adversarial environments.

Keywords
resilience evaluation, combat system of systems, mission capability-inherent capability, wargame simulation

1. Introduction

With the increasing integration of intelligent technologies into military doctrines, the paradigm of modern warfare is shifting from single-platform dominance to multi-domain collaborative combat systems [1–3]. This evolution has given rise to the combat system of systems (CSoS), a new operational form in which decision-making and mission execution are no longer confined to single platforms but require coordinated collaboration across multiple combat units and domains to achieve diverse mission objectives [4,5]. Notably, contemporary CSoS exhibit dual-state characteristics, encompassing mission-active units performing real-time operations and standby units maintaining readiness. Standby

(*) Corresponding author.
E-mail addresses: Y. Sun (ORCID: 0000-0002-7259-1407) dg21150006@smail.nju.edu.cn, Y. Sun (ORCID: 0000-0002-4897-2007) sunyuxiangsun@126.com, Y. Huang, 18534635377@163.com, J. Yu (ORCID: 0009-0000-4565-4217) 18392102175@163.com, X. Zhou (ORCID: 0000-0003-4321-1441) zhouxz@nju.edu.cn

units serve not only as reserves for subsequent missions but also play critical roles in system recovery and replenishment following disruptions. Therefore, effectively incorporating standby units into resilience assessment frameworks has emerged as a critical challenge for comprehensively characterizing the resilience of CSoS.

Since its initial introduction in 1973, resilience has become a fundamental measure of system capability [6–10], widely studied across various domains such as ecological systems [11,12], urban infrastructure [13,14], and engineering systems [15,16]. Given the dynamic nature of battlefield environments, the capability of CSoS inevitably fluctuates or deteriorates under uncertain disruptions, making resilience a key indicator for evaluation and decision-making [17,18]. In this study, we focus on dynamic resilience evaluation of CSoS with mission–standby dual states over long-term confrontations.

Recent studies have begun addressing resilience in military contexts. Sun et al. [19] proposed an extended mission-oriented resilience metric for unmanned weapon system of systems, emphasizing variable mission baselines and recovery times. Jiao et al. [20] employed dynamic Bayesian networks to characterize time-dependent capability evolution, whereas Liu et al. [17] developed the continuous attack resilience index (CARI), considering adaptability and continuous attack scenarios. Chen et al. [21] established a three-stage resilience model addressing resistance, adaptation, and recovery phases. Han et al. [22] proposed a resilience evaluation framework for aerospace defense systems using kill-chain analysis and improved self-information metrics. However, existing resilience assessments focus on constructing complete "resistance-adaptation-recovery" three-stage resilience evolution models, primarily based on closed system assumptions that view standby units as static redundant resources or completely outside the evaluation framework. In realistic confrontations, adversaries often strategically disrupt dynamic transitions between mission-active and standby units, making these existing approaches insufficient for capturing comprehensive dynamic resilience characteristics.

Some progress has been achieved in dynamic resilience research of CSoS. Liu et al. [23] proposed resilience indicators in both performance and time dimensions after disturbances, capturing system evolution during resistance, absorption, and recovery, and characterizing mission requirement completion within mission time. They later extended this line of work to multistate network modeling of unmanned aerial vehicle (UAV) swarms information exchange resilience [24]. Zhu et al. [25] introduced a relative resilience metric for moment-level assessment in dynamic adversarial environments without requiring complete resilience trajectories. However, they still did not consider time-varying attack intensity and strategy evolution resulting from red-blue gaming. Zhang et al. [26] built upon this to propose a dynamic resilience evaluation method applicable to cross-domain collaborative cluster confrontation, using mission unit perception capability as a system resilience indicator to more effectively capture dynamic and uncertain characteristics in system confrontation. The above research on CSoS dynamic resilience analysis primarily focuses on the mission perspective, considering performance evolution modeling based on mission active units while ignoring the potential value of standby units for system capabilities. For example, the UAV swarms resilience measure proposed by Kong et al. [27] indicates that, in comparison to closed-system resource replenishment strategies that significantly enhance swarm performance, standby units inherently possess comparable potential for performance restoration. Zhao et al. [28] further confirmed in balanced system standby pool research that dynamic replacement of components within the standby pool can significantly enhance system expected lifetime and reliability. Evidently, while the explicit performance of mission units determines current operational effectiveness, the potential of standby units affects resilience recovery upper limits. Additionally, current research mainly focuses on evaluating and enhancing system short-term resilience, whereas CSoS often involve large numbers of combat units with long deployment cycles, complex confrontation processes, and multi-stage time-varying mission characteristics [29]. In infrastructure resilience assessment, research has commonly considered the cumulative effects of long-term disturbances and their impact on resilience [30,31]. Therefore, in long-term CSoS confrontations, composite resilience indicators are essential to capture mission units' explicit capabilities and standby units' latent potential. Dynamic assessments should also set phase-specific thresholds and goals to avoid transition distortions, as phases require distinct capabilities (e.g., detection emphasizes

perception and survivability; strikes prioritize delivery and effectiveness). Fixed thresholds risk false losses in low-demand phases or overstated resilience in high-demand ones. Supported by mission-oriented studies (e.g., [19,25,32]), adaptive thresholds ensure comparability. These needs highlight the refinement of CSoS frameworks by integrating standby potential and enhancing multi-phase accuracy.

Current mission unit resilience measurements typically focus on explicit performance representations during mission execution, such as awareness capabilities, communication connectivity, and motion attributes. However, there remains a lack of suitable indicators for standby unit resilience measurement in CSoS. Existing system resilience indicator selection spans multiple dimensions: from a system structure perspective, Henry et al. [33] suggested integrating key parameters including disruptive events, recovery strategies, and overall resilience strategies. Uday et al. [34,35] constructed system importance metrics based on component system impact analysis. Watson et al. [36,37] developed a resilience measurement methodology combining System of Systems (SoS) dynamics models. Complex network topological property indicators (e.g., connectivity [38], maximum flow [39], and meta-path-based measures [40]) are widely used to characterize combat-network structure and robustness, providing useful structural evidence for resilience assessment [41]. In performance evolution-based measurement methods, Chen et al. [42] constructed performance threshold-driven resilience indicators through hierarchical decomposition of combat systems. Tran et al. [43] evaluated resilience under multi-stage disruption by comparing changes in information transfer node quantities before and after system disturbance. Bai et al. [32] introduced UAV swarms performance deviation from benchmark systems as an improved indicator based on the Tran framework. Zhong et al. [44] quantified unmanned combat system of systems resilience from mission benefit and performance fluctuation dimensions. Additionally, Kong et al. [27] proposed a UAV group resilience measurement model integrating system structure and mission chain performance, while Feng et al. [45] achieved multi-scale characterization of system states by constructing a three-dimensional indicator cube encompassing length, height, and width. For in long-term confrontation of CSoS overall capability research, there remains a need to construct composite resilience indicators that can simultaneously characterize both the explicit capabilities of system mission units and the potential capabilities of standby units.

To address the challenges in evaluating the dynamic resilience of CSoS with mission-standby dual states in long-term confrontation, this paper proposes a dual-dimensional resilience evaluation framework. By analyzing the dynamic gaming mechanism in confrontation processes, we propose a composite resilience indicator that integrates standby units' inherent performance based on existing mission-oriented resilience measurement frameworks. Additionally, a dynamic phase-segmented resilience evaluation model (DPS-RE) is developed, leveraging time-varying performance baselines to maintain evaluation sensitivity across prolonged confrontations. To verify the model's effectiveness, this research constructs simulation experiments to quantitatively analyze how standby unit performance inhibits rapid CSoS capability deterioration, revealing the differentiated impact of different capability unit replenishment strategies on combat capability enhancement through multi-dimensional resilience curves. Further based on multi-domain joint operations simulation cases, this study analyzes the dynamic attenuation patterns of both sides' resilience in long-term gaming and examines the applicability of the evaluation model in realistic combat scenarios. The key contributions of this study are summarized as follows:

(1) A dual-dimensional resilience evaluation framework, integrating mission capability and inherent capability, is proposed. This framework combines the survival probabilities of mission-active units with the perception and strike capabilities of standby units, providing comprehensive coverage of all units within the mission-standby CSoS. It enables simultaneous quantitative characterization of both instantaneous combat capability and latent recovery potential, thus supporting refined decision-making in dynamic confrontation scenarios.

(2) We designed a dynamic phase-segmented resilience evaluation model (DPS-RE) to overcome the limited adaptability of existing evaluation models in long-term confrontations. The model identifies disturbance event stage characteristics and combines time-varying performance baselines with dynamic expectation

thresholds to construct a multi-phase resilience evolution analysis model, effectively mitigating evaluation sensitivity degradation caused by time accumulation effects.

(3) Simulation experiments demonstrate the time-dependent mechanisms by which standby unit failures and dynamic resource replenishment influence system resilience degradation. Through multi-domain joint operations case studies, the dynamic adaptability of the proposed DPS-RE model is validated for capability assessment of CSoS in prolonged confrontations. The proposed framework effectively supports decision-making regarding mission adjustments and resource allocation in adversarial environments.

The remainder of this paper is organized as follows: Section 2 describes CSoS dynamic processes and performance curves incorporating standby units. Section 3 proposes multi-dimensional indicators for confrontations with standby units and an improved multi-phase resilience method. Section 4 presents illustrative experiments verifying feasibility and effectiveness. Section 5 analyzes red and blue resilience variations using multi-domain simulation data and provides recommendations. Section 6 summarizes findings and outlines future research.

2. Combat system of systems confrontation process description

In long-term confrontation scenarios, dynamic resilience assessment for CSoS must overcome the limitations inherent in single-dimensional, mission capability-oriented approaches. To address this, we introduce a dynamic adversarial-interaction description of CSoS confrontations, analyze the evolution patterns of combat units exhibiting dual-state ("mission-active" and "standby") characteristics, and elucidate the dual contributions of standby units in both mission execution and overall CSoS recovery.

2.1. Analysis of CSoS Confrontation Process

The confrontation process of CSoS typically involves three sequential stages: deployment, confrontation, and termination [46,47]. In the deployment stage, each side conducts initial mission planning for various multi-domain combat units, including airborne aircraft, ground-based armored units, surface vessels, and underwater submersibles. This planning adheres to multi-domain collaboration principles, encompassing tactical missions such as patrol, interference, defense, and strike operations. The subsequent confrontation stage follows Boyd's Observe-Orient-Decide-Act (OODA) loop model [48–50], characterized specifically by real-time perception through multi-domain sensors identifying enemy unit types, numbers, and intentions (depicted as blue information flow in Fig. 1. Decision centers fuse the collected situational information and issue dynamic mission instructions (red decision feedback flow in Fig. 1). Combat units then execute these instructions and simultaneously transmit effectiveness data, forming iterative closed-loop cycles. In the final termination stage, confrontation outcomes are determined based on the degree of mission objective achievement.

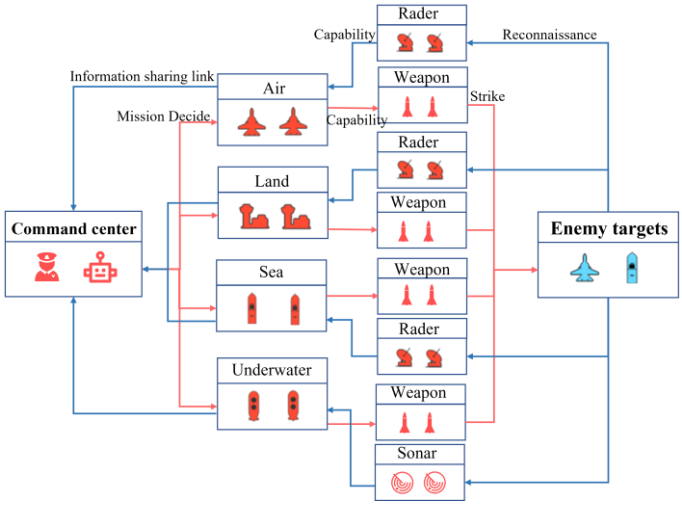

Figure 1. Illustration of CSoS dynamic process.

The confrontation stage exhibits long-duration characteristics with multi-mission asynchronous execution and dynamic adversarial interactions, causing combat units to exist in three possible states: inactive (standby), mission-active, and mission-terminated. Taking stage T in Fig. 2 as an example, only the green-colored units are engaged in active missions, while gray-colored units remain in standby status. By stage $T+k$, losses of mission-active units trigger the activation mechanism of standby units. At stage $T+n$, standby units face potential risks of adversarial attacks, and their performance deterioration directly influences overall CSoS resilience. Therefore, resilience assessment frameworks must comprehensively integrate the dynamic operational effectiveness of mission-active units and the inherent

availability of standby units.

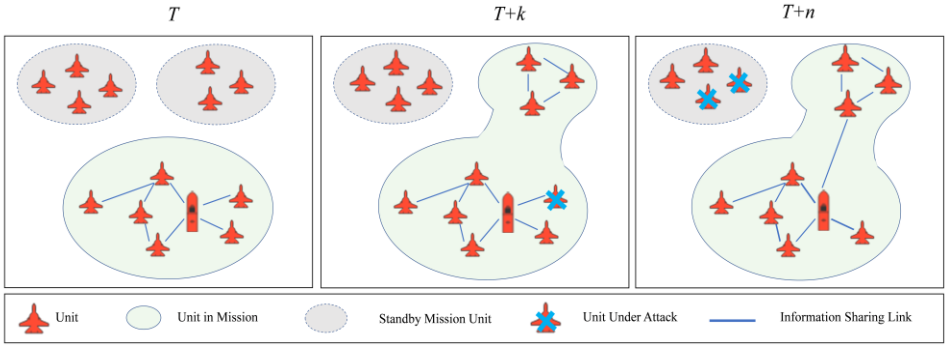

Figure 2. "Mission-Standby" states of combat units.

2.2. CSoS performance curves incorporating standby units

Current resilience assessment frameworks for CSoS mainly focus on the performance evolution of mission-active units [25,51]. Typical performance curves (green curve in Fig. 3(b)) evaluate resilience based on survival rates derived from multi-dimensional operational attributes (e.g., angle, speed, distance). However, they overlook the latent contributions of standby units—such as reconnaissance coverage and potential strike capabilities—to overall resilience (blue curve in Fig. 3(b)). To address this, we propose a dual-dimensional framework that integrates both mission capability and inherent capability.

Definition 1 — Mission Capability ($Q_{mission}$): The real-time, dynamic performance of mission-active units during operational engagements. It is quantified through operational attributes such as perception, maneuverability, and strike capability, directly reflecting the immediate combat effectiveness and sustained operational ability of the CSoS.

Definition 2 — Inherent Capability ($Q_{Inherent}$): $Q_{Inherent}$ denotes the mobilizable potential of the remaining CSoS asset pool (active and standby), characterized by residual resources, redundancy and substitutability. It represents the structural capacity that constrains the achievable mission performance over time. In general, the realized mission performance is bounded by the available inherent resources, i.e., $Q_{mission}(t)$ is limited by $Q_{inherent}(t)$. The two curves may respond differently to the same disruption because $Q_{mission}(t)$ depends on the current active configuration, whereas $Q_{inherent}(t)$ depends on the residual assets and their mobilizability.

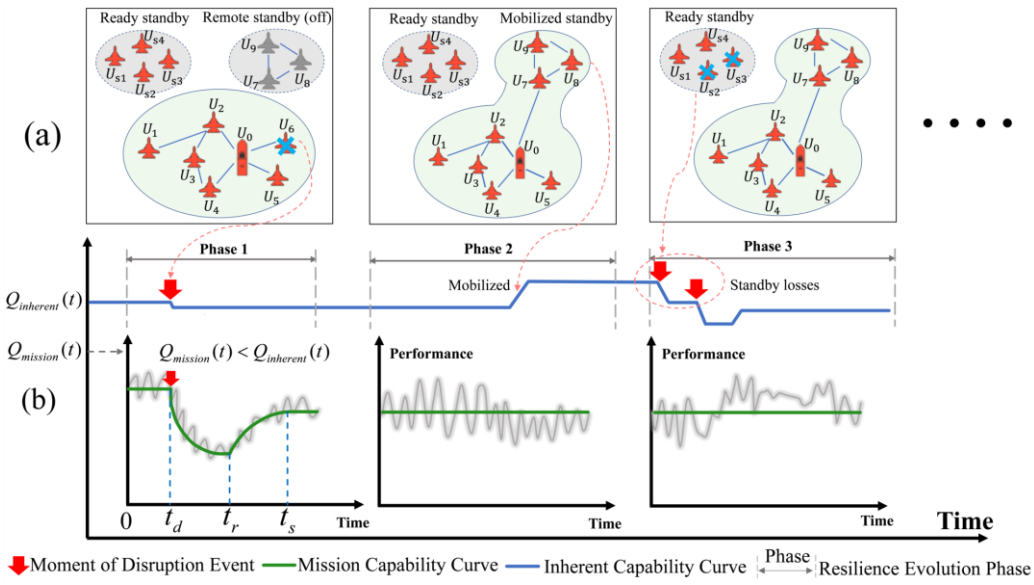

Figure 3. Comparative illustration of CSoS resilience curves integrating mission and inherent capability dimensions.

Fig. 3 comparatively illustrates resilience assessment perspectives: panel (a) depicts CSoS disruption scenarios in long confrontation cycles, with Phase 1 showing attacks on mission-active units (e.g., U_6) while some remote standby units remain temporarily unavailable ("standby (off)"), Phase 2 illustrating adaptation and recovery through standby

mobilization (e.g., remote standby switching to "mobilized standby"), and Phase 3 demonstrating continuous losses to standby units (e.g., U_{s1} and U_{s2}); panel (b) shows the corresponding performance evolution integrating mission capability ($Q_{mission}(t)$, achieved mission performance of active units) and inherent capability ($Q_{inherent}(t)$, mobilizable potential of the remaining asset pool including both active and standby units). In long-term confrontations with uncertain disruption timings, individual impacts may overlap; by adapting Tran's multi-epoch assessment theory [43] and introducing dynamic phase-identification criteria, we treat overlapping disruptions as unified compound phases (e.g., Phase 3 in Fig. 3(b)), reducing fragmented epochs and avoiding double-counting to improve the robustness and consistency of resilience evaluation.

3. Dynamic resilience model under confrontation

Based on the dynamic resilience curve analysis presented in Section 2, the inherent capabilities of standby units significantly influence CSoS resilience recovery during long-term confrontations. Unlike existing methods that solely model resilience through the performance degradation of mission-active units, we propose a dual-dimensional resilience assessment framework that integrates both mission and inherent capabilities. This approach provides precise quantitative support for mission planning and resource replenishment within CSoS.

3.1. CSoS performance indicators

3.1.1. Mission capability quantification indicators

We adopt the mission-capability evaluation framework in Zhang et al. [26] with two adjustments. First, we redefine the angle perception $c\alpha_{ij}(t)$ using heading angles that are consistently available across heterogeneous platforms in our simulations. Second, we revise the unit-level survivability aggregation $SU_i(t)$ across multiple perceived enemies to a conservative worst-case form, while the remaining terms and weighting structure follow [26]. Let i denote a mission-active friendly unit and j denote an enemy unit. Let $\theta_i(t)$ and $\theta_j(t)$ be their heading angles, $v_i(t)$ and $v_j(t)$ be their speeds, and $D_{ij}(t)$ be the Euclidean distance between them at time t. Let R_s and R_a denote the perception range and attack range of unit i, respectively. Let $C_i(t)$ be the set of enemy units within the perception range of unit i at time t.

The angle perception between unit i and enemy unit j is defined in Eq. (1) as:

$$c\alpha_{ij}(t) = 1 - \frac{\Delta\theta}{\pi} \tag{1}$$

where $\Delta\theta = min(|\theta_i - \theta_j|, 2\pi - |\theta_i - \theta_j|)$.

Fig. 4 illustrates the parameters and the calculation of the angle perception indicator.

The velocity perception follows [26] and is given in Eq. (2) as a piecewise function of the speed ratio $v_i(t)/v_j(t)$.

$$cv_{ij}(t) = \begin{cases} -1, & \frac{v_i(t)}{v_j(t)} < 0.5 \\ 1, & \frac{v_i(t)}{v_j(t)} \geq 1.5 \\ 2 \cdot \frac{v_i(t)}{v_j(t)} - 2, & \text{otherwise} \end{cases} \tag{2}$$

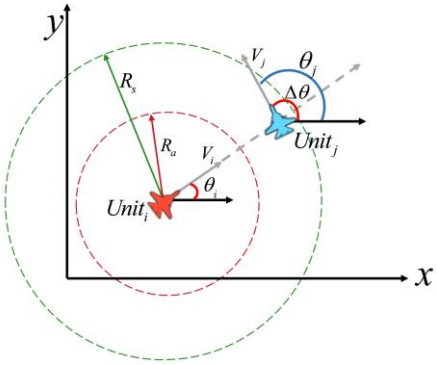

Figure 4. Calculation of angle perception indicator.

Given that $c\alpha_{ij}(t) \in [0,1]$, the distance perception is defined in Eq. (3) as:

$$cd_{ij}(t) = c\alpha_{ij}(t) \cdot \left[1 - \frac{D_{ij}(t) - R_a}{R_s - R_a}\right] \tag{3}$$

The pairwise survivability score of unit i against enemy j is computed in Eq. (4) as:

$$S_{ij}(t) = \beta_a c\alpha_{ij}(t) + \beta_d cd_{ij}(t) + \beta_v cv_{ij}(t) \tag{4}$$

where $\beta_a, \beta_d, \beta_v \geq 0$ and $\beta_a + \beta_d + \beta_v = 1$ .To conservatively account for multiple threats, the survivability indicator of unit i is determined by the most threatening enemy, as defined in Eq. (5):

$$SU_i(t) = \min_{j \in C_i(t)} S_{ij}(t) \tag{5}$$

Finally, the CSoS mission capability is obtained by aggregating the survivability indicators of all mission-active units, as in Eq. (6):

$$Q_{mission}(t) = \sum_{i=1}^{N_0(t)} S\,U_i(t) \tag{6}$$

where N_0 denotes the number of mission-active units at time t, updated dynamically as units switch operational states.

3.1.2. Inherent capability quantification indicators

Based on Boyd's Observe Orient Decide Act loop, the inherent capability of a CSoS should support Observe, Decide, and Act (Fig. 1). Here, we characterize inherent capability through measurable outcomes in two components, multi-domain reconnaissance capability and multi-domain strike potential, which together capture the system's latent capacity for sustaining and recovering effectiveness under disruption.

(1) Multi-domain Reconnaissance Index

In dynamic confrontation, multi-domain combat units achieve full-domain situation awareness through heterogeneous sensor networks. Detection range directly determines the spatial coverage of the CSoS's "Observe" capability and forms the physical basis of the OODA loop.

Let unit i be equipped with a set of sensors $\mathcal{D}_i$, and let $K_i = |\mathcal{D}_i|$ denote the number of sensors on unit i. For each sensor $d_{i,k} \in \mathcal{D}_i$, let $r_{i,k}^{max}$ denote its theoretical maximum detection radius, and let $e_{i,k}(t) \in \{0,1\}$ denote its activation state at time t, where 1 indicates active and 0 indicates inactive. The effective detection radius of unit i at time t is defined as the maximum detection radius among activated sensors.

$$r_i(t) = max\{e_{i,k}(t) \cdot r_{i,k}^{max} \mid d_{i,k} \in \mathcal{D}_i\} \quad (7)$$

At the CSoS level, let N denote the total number of units, and let $\delta_i(t) \in \{0,1\}$ indicate whether unit i is equipped with reconnaissance sensors (capability indicator). Let $N_u = \sum_{i=1}^{N} \delta_i$ denote the number of sensing-capable units. We then define the CSoS-level reconnaissance index as the mean effective detection radius over sensing-capable units. This formulation captures the overall sensing scale of the system while remaining compatible with dynamic confrontation modeling. Under spatially dispersed deployment, the observable space increases with detection radii, making the averaged effective radius a practical approximation of spatial coverage.

$$C_{obs}(t) = \frac{1}{N_u} \sum_{i=1}^{N} \delta_i \cdot r_i(t) \quad (8)$$

To enable fusion with strike potential despite differing physical units, we further use a dimensionless form normalized by the pre-disruption baseline.

$$\tilde{C}_{obs}(t) = \frac{C_{obs}(t)}{C_{obs}(T_0)} \quad (9)$$

where T_0 denotes the baseline time immediately before the disruption phase.

(2) Multi-domain Strike Potential Index

Standby units within a CSoS, despite not actively engaging in current missions, inherently maintain latent strike capabilities against targets in multiple operational domains, including air, sea, land, and underwater environments. To quantify this latent capability, we define the strike potential index $C_{act}(t)$ for each unit i.

The strike potential of a combat unit i at time t against targets in domain $m \in \{air, land, sea, underwater\}$ is defined as:

$$A_i^{(m)}(t) = \delta_i^{(m)}\left[W_i^{(m)}(t) \cdot R_i^{(m)} \cdot P_i^{(m)}\right] \quad (10)$$

where $\delta_i^{(m)} \in \{0,1\}$ indicates whether unit i possesses strike capability in domain m (1 if capable, 0 otherwise), $W_i^{(m)}(t)$ denotes the number of available weapon resources for unit i against domain m targets at time t, considering prior weapon usage and resource depletion, $R_i^{(m)}$ is the effective combat radius of unit i against domain m targets, and $P_i^{(m)}$ is the probability of successful engagement (single-strike damage probability) of unit i against domain m targets, obtainable from historical data or simulation results.

The overall CSoS-level strike potential $C_{act}(t)$ is then calculated by aggregating individual unit capabilities across all operational domains:

$$C_{act}(t) = \sum_m \omega_m(t) \cdot \left(\sum_{i=1}^{N} A_i^{(m)}(t)\right) \quad (11)$$

where the weight coefficient $\omega_m(t)$ is determined by the proportion of effective units in each domain relative to the total effective units, calculated as follows:

$$\omega_m(t) = \frac{N_m(t)}{\sum_{m'} N_{m'}(t)} \quad (12)$$

where $N_m(t)$ denotes the number of effective units in domain m at time t.

Similarly, to ensure comparability for fusion, we use the dimensionless form:

$$\tilde{C}_{act}(t) = \frac{C_{act}(t)}{C_{act}(T_0)} \quad (13)$$

We define inherent capability as a fusion of the dimensionless observation proxy and strike potential:

$$Q_{inherent}(t) = \Gamma(\tilde{C}_{obs}(t), \tilde{C}_{act}(t)) \quad (14)$$

where $\Gamma(\cdot)$ denotes a dynamic fusion operator that adaptively adjusts the weights between reconnaissance and

strike capabilities according to evolving confrontation phases. The operator is formalized as a weighted linear combination:

$$Q_{inherent}(t) = \alpha(t) \cdot \tilde{C}_{\text{obs}}(t) + (1 - \alpha(t)) \cdot \tilde{C}_{\text{act}}(t) \quad (15)$$

The weight $\alpha(t) \in [0,1]$ adapts to the confrontation phases, reflecting the varying emphasis on reconnaissance and strike capabilities based on the CSoS's mission requirements. To obtain reproducible and stable weight updates, $\alpha(t)$ is constrained away from the degenerate endpoints 0 and 1. We define:

$$\alpha(t) = max(\alpha_{min}, min(1 - \alpha_{min}, 0.5 + \lambda \cdot (I_{\text{recon}}(t) - I_{\text{strike}}(t)))) \quad (16)$$

where $\alpha_{min} > 0$ prevents single-indicator dominance under noisy estimates, $\lambda \in [0,0.5]$ is a sensitivity coefficient. The mission intensities are defined as $I_{\text{recon}}(t) = N_{\text{recon}}(t)/N(t)$ and $I_{\text{strike}}(t) = N_{\text{strike}}(t)/N(t)$, where $N_{\text{recon}}(t)$ and $N_{\text{strike}}(t)$ are the numbers of reconnaissance and strike units at time t, and $N(t)$ is the total number of units in the CSoS. Some units undertake both reconnaissance and strike roles and are therefore counted in both categories.

The adaptive mechanism ensures that the weight responds to operational priorities, such as $\alpha(t)$ increasing above 0.5 when reconnaissance capabilities are dominant (e.g., in close-range surveillance phases), decreasing below 0.5 when strike capabilities are dominant (e.g., in interception missions), and remaining at 0.5 when reconnaissance and strike requirements are balanced.

3.2. Dynamic resilience calculation method

3.2.1. Dynamic resilience framework

The dynamic resilience of a system based on mission capability can be comprehensively assessed through two dimensions: time resilience and performance resilience. Following the research framework developed by Liu [23] and Zhang [26], the mission capability resilience $Re_{mission}(t)$ is expressed as:

$$Re_{mission}(t) = \beta \cdot Re_0(t) + (1 - \beta) \cdot Re_1(t) \quad (17)$$

where β $(0 \leq \beta \leq 1)$ is a weighting factor. Specifically, time resilience $Re_0(t)$ denotes the proportion of continuous time during which the performance of the system's mission units remains above a predefined minimum threshold $Q_{min}(t)$, calculated as:

$$Re_0(t) = \frac{\int_{T_0}^{t} [(Q(t) - Q_{min}(t) \geq 0)]dt}{t - T_0} \quad (18)$$

The performance resilience $Re_1(t)$ captures the recovery efficiency of actual mission unit performance relative to an optimal performance level $Q_{opt}(t)$:

$$Re_1(t) = \frac{\int_{T_0}^{t} Q(t) \cdot [(Q(t) - Q_{min}(t) \geq 0)]dt}{\int_{T_0}^{t} Q_{opt}(t)dt} \quad (19)$$

Although the theoretical definition of these resilience indicators employs continuous integration, actual combat scenarios typically yield discrete data. Data concerning mission and inherent capabilities are generally collected via sensor networks or simulations at discrete intervals Δt, forming discrete-time series $\{Q_{inherent}(k)\}_{k=1}^{K_T}$,where K_T is the number of sampled time steps. Accordingly, we adapt the dynamic resilience calculation structure defined in Eq. (17) for the inherent capability dimension, denoted $Re_{inherent}$, using discrete formulations. Thus, discretized forms of time resilience $Re_0'(t)$ and performance resilience $Re_1'(t)$ are defined as follows:

- Discrete-time resilience:

$$Re_0'(t) = \frac{\sum_{k=T_0}^{t} \mathbb{I}_{\{Q_{\text{inherent}}(k) \geq Q_{min}(k)\}}}{t - T_0 + 1} \quad (20)$$

- Discrete-performance resilience:

$$Re_1'(t) = \frac{\sum_{k=T_0}^{t} Q_{\text{inherent}}(k) \cdot \mathbb{I}_{\{Q_{\text{inherent}}(k) \geq Q_{min}(k)\}}}{\sum_{k=T_0}^{t} Q_{\text{opt}}(k)} \quad (21)$$

Here, $Q_{min}(t)$ denotes the minimum performance threshold required at time t, and $Q_{opt}(t)$ represents the theoretically optimal performance achievable by the CSoS.

The determination of $Q_{min}(t)$ is grounded in mission-criticality analysis to capture evolving strategic priorities. For instance, mission requirements may stipulate that the CSoS's sensing capability must be sustained at no less than 80% of its initial level, whereas its strike capability must remain above 60%. Formally, this is expressed as $Q_{min}^{j}(t) = Q_{initial}^{(j)}(t) \times \eta_j$, ,where$Q_{initial}^{(j)}(t)$ denotes the pre-disruption capability for dimension j, and η_j is a mission-criticality adjustment factor determined through historical data or expert judgment. The indicator function $\mathbb{I}_{\{Q_{inherent}(k) \geq Q_{min}(k)\}}$ equals 1 if the inherent capability meets or exceeds the threshold and 0 otherwise.

Consequently, the dynamic resilience of the CSoS is independently quantified in a dual-dimensional framework, incorporating both mission capability and inherent capability, as shown in Eq. (22):

$$Re_{SoS}(t) = [Re_{mission}(t), Re_{inherent}(t)]^T \quad (22)$$

This independent quantification strategy is adopted because,

from a practical command and control perspective, mission capability primarily relates to real-time situational maintenance, while inherent capability corresponds to resource scheduling and planning. Maintaining dimensional independence between these resilience indicators provides decision-makers with nuanced insights, facilitating precise cognitive differentiation between immediate combat effectiveness and long-term resource availability.

3.2.2. Dynamic phase-segmented resilience evaluation (DPS-RE)

To address the limitations of continuous time-resilience evaluation (CT-RE) in long-duration confrontations with multiple disruptions, we propose a dynamic phase-segmented resilience evaluation (DPS-RE) scheme. Following the multi-disruption assessment idea of Tran et al. [42], DPS-RE partitions the confrontation timeline into event-centered phases and evaluates resilience phase by phase. The procedure is summarized as follows.

Step 1: Phase division based on disruption events.

We utilize the occurrence of disruption events as the fundamental criterion for defining phases. Specifically, the entire confrontation cycle $\mathcal{T}$ is segmented into k dynamic phases:

$$\mathcal{T} = \{E_1, E_2, \cdots, E_k\} \tag{23}$$

Each phase E_i is defined by a time window centered at the i-th disruption event time T_i,

$$E_i = [T_i - \Delta T_0(i), T_i + \Delta T_1(i)) \tag{24}$$

Here, $\Delta T_0(i)$ and$\Delta T_1(i)$ denote the pre-event and post-event observation windows. They are determined from the local spacing of disruption events so that windows shrink under clustered disruptions and expand under sparse disruptions. Specifically, we set $\Delta T_0(i)$ proportional to the preceding inter-event interval and $\Delta T_1(i)$ proportional to the following interval, with a single scaling factor κ. Both windows are bounded within $[\Delta T_{min}, \Delta T_{max}]$ to avoid pathological fragmentation or excessive expansion. This ensures that each identified phase captures a complete disruption–adaptation–recovery cycle consistent with the operational rhythm of the confrontation.

Step 2: Phase merging strategy.

If adjacent candidate phases overlap, i.e., $T_i - \Delta T_0(i) \leq T_{i-1} + \Delta T_1(i-1)$, the corresponding phases are merged into a unified phase:

$$E_{new} = [min(T_{i-1} - \Delta T_0(i-1), T_i - \Delta T_0(i)), max(T_{i-1} + \Delta T_1(i-1), T_i + \Delta T_1(i))] \tag{25}$$

This merging step avoids ambiguity caused by overlapping disruption and recovery intervals and prevents double counting when multiple events occur within a short time span (as illustrated in Fig. 3(b)). After merging, the resulting phases are ordered and non-overlapping, preserving time continuity over the entire horizon.

The final CSoS-level resilience for the entire confrontation period is represented by an aggregated set of resilience vectors for each identified phase:

$$Re_{SoS} = \{Re_{SoS}^{E_1}, Re_{SoS}^{E_2}, \ldots, Re_{SoS}^{E_n}\} \tag{26}$$

where each phase-specific resilience measure $Re_{SoS}^{E_i}$ is computed according to Eq. (22), applying distinct minimum performance thresholds Q_{min} and optimal performance values Q_{opt} adjusted dynamically to the specific conditions of each phase.

The detailed pseudocode implementation of this method is provided in Algorithm 1.

Algorithm 1 Multi-phase resilience calculation

Input: Disruption event times $\{T_1, T_2, \ldots, T_m\}$;parameters $\kappa, \Delta T_{min}, \Delta T_{max}$

Output: Multi-phase resilience set $\mathscr{R}$

Initialize: $\mathscr{E} \leftarrow \emptyset, \mathscr{R} \leftarrow \emptyset$
$\tilde{d} \leftarrow \text{median}(\{T_i - T_{i-1}\}_{i=2}^{m})$
for $i = 1$ to m **do**
  $d^- \leftarrow (T_i - T_{i-1})$ if $i > 1$, else $\tilde{d}$
  $d^- \leftarrow (T_{i+1} - T_i)$ if $i < m$, else $\tilde{d}$
  $\Delta T_0(i) \leftarrow \min(\Delta T_{max}, \max(\Delta T_{min}, \kappa d^-))$
  $\Delta T_1(i) \leftarrow \min(\Delta T_{max}, \max(\Delta T_{min}, \kappa d^+))$
  Generate initial epoch: $E_i = [T_i - \Delta T_0(i),\ T_i + \Delta T_1(i))$
  $\mathscr{E} \leftarrow \mathscr{E} \cup \{E_i\}$
end for
While overlapping epochs exist **do**
  Merge overlapping epochs E_j, E_k intoE_{merged}
  Update$\mathscr{E} \leftarrow (\mathscr{E} \setminus \{E_j, E_k\}) \cup E_{\text{merged}}$
end while
for each epoch $E_i \in \mathscr{E}$ **do**
  Calculate $Re_{\text{SoS}}^{E_i}$via Eq.~(22)
  Update $\mathscr{R} \leftarrow \mathscr{R} \cup \{Re_{\text{SoS}}^{E_i}\}$
end for
Return $\mathscr{R}$

3.2.3. CSoS dynamic resilience assessment step

Based on the proposed performance indicators and dynamic resilience model, we establish a structured workflow to evaluate CSoS resilience under confrontation. As summarized in Fig. 5, the procedure consists of four steps.

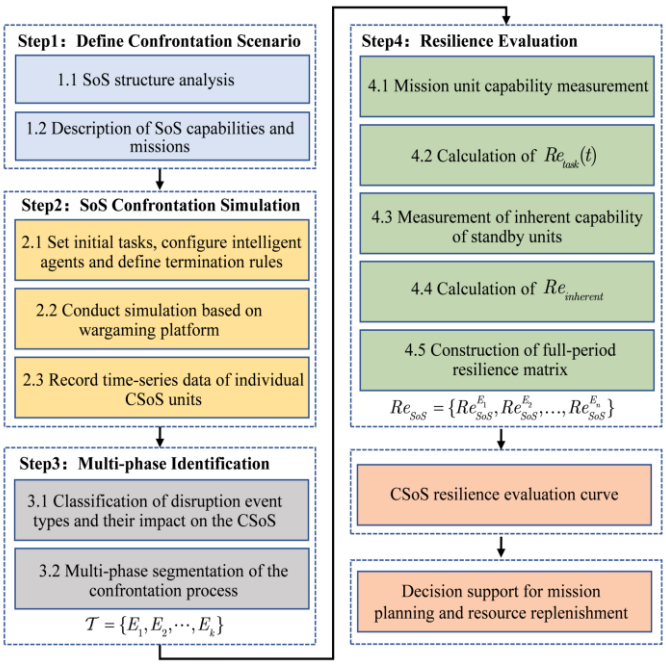

Figure 5. CSoS dynamic resilience assessment method block diagram.

(1) Confrontation Scenario Construction. Multi-domain scenarios for red and blue CSoS are built using historical or hypothesized data, including system architectures, unit configurations, mission sets, unit mission-capability mapping matrices, and performance threshold vectors as inputs for wargaming simulations.

(2) Combat Simulation. Using the Mozi platform, confrontation processes are simulated with initialized agent parameters, mission planning, termination criteria, and time dynamics modeling. Damage event logs and unit performance parameters are recorded.

(3) Phase identification. Confrontation phases are extracted from disruption events in the simulation logs. Event-centered candidate windows are generated with adaptive observation horizons, and temporally overlapping windows are merged to obtain the final phase set $\mathcal{T} = \{E_1, E_2, \cdots, E_k\}$.

(4) Dual-dimensional resilience evaluation. For each phase, resilience is quantified along two independent dimensions, namely mission capability resilience $Re_{misssion}$ and inherent capability resilience $Re_{inherent}$. The confrontation-level output is a phase-wise resilience set $\{Re_{SoS}^{E_1}, Re_{SoS}^{E_2}, \ldots, Re_{SoS}^{E_n}\}$

Finally, the resulting resilience trajectories support operational recommendations such as time-critical mission adjustments and resource replenishment planning.

4. Illustrative experiments

4.1. Experiment description

To verify the effectiveness of the proposed dynamic resilience model, this research constructed a typical red-blue CSoS confrontation scenario and implemented confrontation simulation through the Mozi wargame platform (http://www.hs-defense.com/). The combat unit configurations for both sides are shown in Table 1. This simulation experiment mainly verifies the impact of standby unit performance on CSoS resilience assessment, therefore fewer disruption events can be treated as a single phase. The simulation termination rule is set to either side's combat unit loss score reaching 200 points or the simulation duration exceeding 1000 time steps.

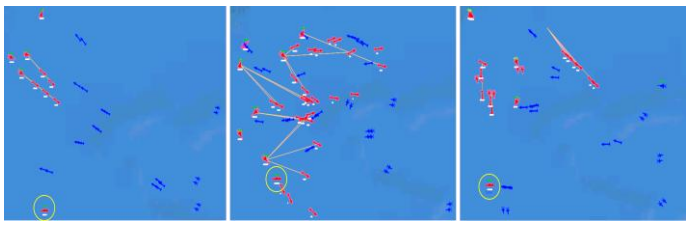

Figure 6. Simulation process of system confrontation.

Fig. 6 shows the CSoS confrontation simulation process, with the red side's Sea unit in the yellow circle serving as a CSoS standby unit, while all other units participate in real-time combat missions.

Table 1. Unit types and quantities of red and blue sides.

Side	Unit Type	Number of Units	Number of Initial Missions
Red Side	Air Units	12	2
	Sea Units	1	
Blue Side	Air Units	16	3

Note: "Number of Initial Missions" represents the total initial missions assigned to each side at simulation onset.

In the simulation process, three types of core data are recorded including detection perception data, unit status data, and mission action data, with specific attributes for each type listed in Table 2. Disruption events were extracted from the Mission Action data by examining the Task Result attribute.

A disruption event is registered when a red-side unit receives a confirmed "KILL" result, indicating unit destruction. Based on this rule, three key disruption events were identified at t = 500, 513, and 533 (Table 3).

Table 2. Attributes of combat data.

Data Name	Attributes
Detection & Perception	Time, Unit Side, Sensor Id, Sensor ParentId, Detection Mode, Detection Range, Target Course, Target Longitude, Target Latitude, Target Range, Target Altitude, Target Speed, Detection Result.
Unit Status	Time, UnitID, Unit Longitude, Unit Latitude, Unit Type, Course, Speed, Operational Mission, Detection Range, Fire Range.
Mission Action	Time, WeaponID, Weapon Side, Parent Firing UnitID, TargetID, Target Longitude, Target Latitude, Task Result.

Table 3. Lost units and their status in the red side.

Time of Attack	The attacked units	Mission Status
500	U_S^1	Mission Not Activated
513	U_A^4	In Mission
533	U_A^6	In Mission

4.2. Resilience quantification considering standby units

Fig. 7 compares the dynamic evolution of CSoS mission capability ($Q_{misssion}$) and inherent capability ($Q_{inherent}$) under disruption events. Regarding inherent capability sensitivity, Fig. 7(a) indicates significant reductions in detection perception ($Q_{inherent1}$) and strike potential ($Q_{inherent2}$) at t =500 due to the loss of standby unit U_S^1. Subsequent mission unit losses at t =513,533 further degraded inherent capabilities, demonstrating inherent capability's sensitivity to losses across all CSoS units.

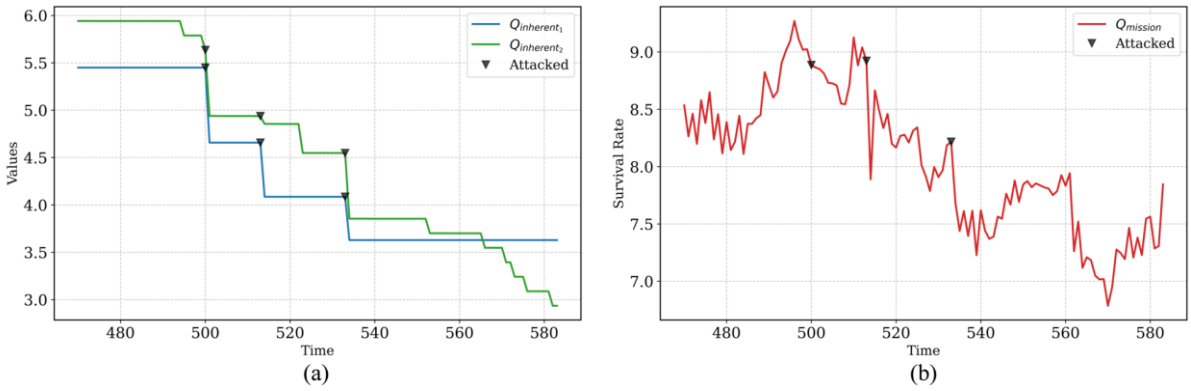

Figure 7. Evolution of CSoS inherent capability and mission capability under disruption events.

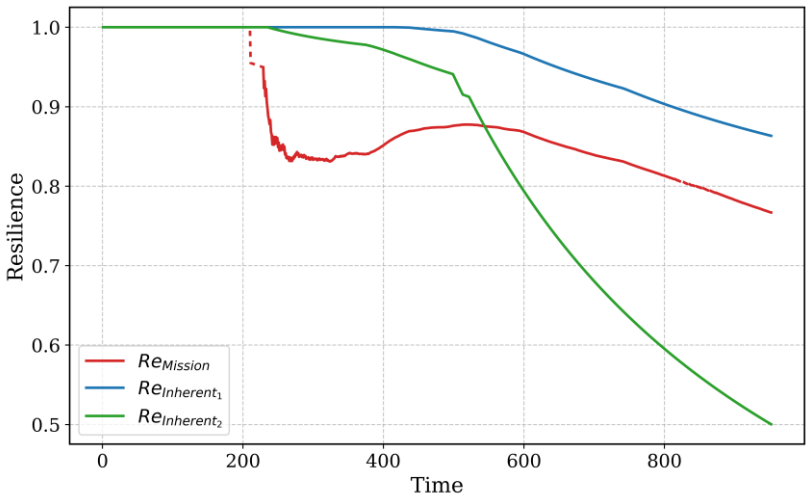

Figure 8. Dual-dimensional dynamic resilience curve of the CSoS.

In contrast, Fig. 7(b) illustrates CSoS performance changes following the single-dimension, mission-oriented approach of existing reference [26]. The $Q_{misssion}$ curve exhibits clear sensitivity only to losses of mission-active units at t =513,533, while the destruction of standby units at t =500 is less discernible. For dual-state CSoS featuring mission-active and standby units, reliance solely on mission-active unit performance overlooks the latent combat potential of standby

units. This omission creates perception blind spots, limiting a comprehensive understanding of overall CSoS resilience.

Further comparison of resilience assessments across both mission capability and inherent capability dimensions is depicted in Fig. 8. Using 65% of the initial performance as the baseline, the mission capability resilience curve (red line) maintains resilience above 0.75 throughout the mid-to-late confrontation stages, suggesting high system resilience. However, the inherent capability resilience curve (green line), incorporating standby units and resource depletion, falls below the baseline after t =732, indicating that actual system recovery potential is insufficient for prolonged combat. Thus, traditional single-dimension evaluations tend to overestimate resilience, potentially misleading decision-makers. The dual-dimension approach, by separately quantifying real-time effectiveness and available capability, offers a more precise analytical basis for strategic command decisions.

4.3. Discussion

4.3.1. Impact of standby units on CSoS resilience

To further explore the relationship between the number of standby units and overall CSoS resilience, we conducted comparative experiments in which the red side's standby units increased from 1 (U_S^1) to 6 ($U_S^1 \ldots U_S^6$), with incremental destruction of 2, 4, and 6 standby units at t =500. Fig. 9 presents the resulting resilience calculations.

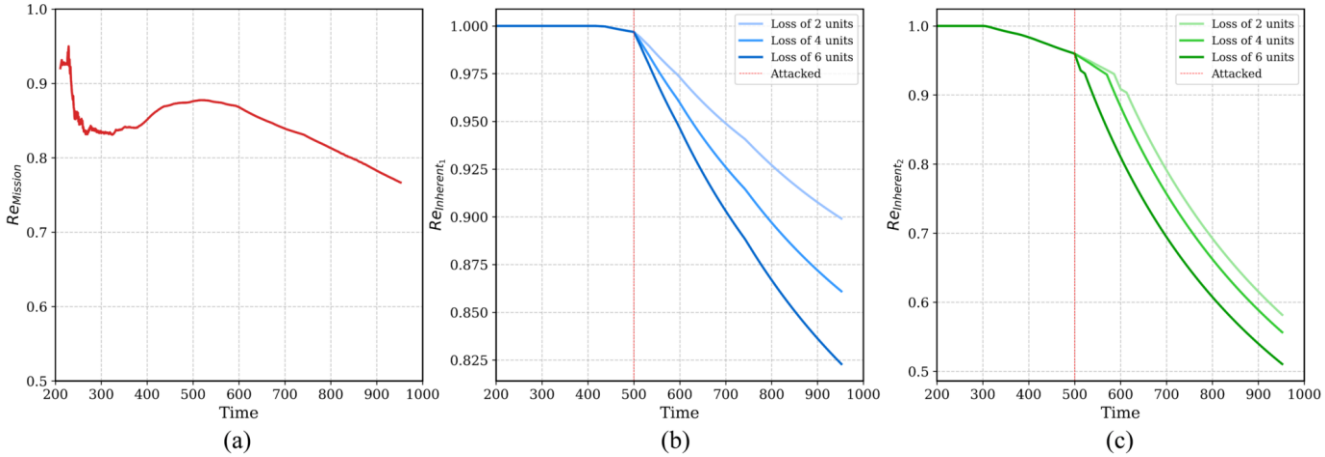

Figure 9. CSoS resilience trends under varying levels of standby unit loss.

Fig. 9(a) indicates that resilience assessed via mission capability remains insensitive to increasing standby unit losses, exposing inherent limitations in single-dimensional evaluation models.

Fig. 9(b) and (c), however, illustrate resilience calculations based on inherent capability. Unlike the mission capability approach, inherent capability indicators effectively capture the total reconnaissance perception and available strike reserves, offering a comprehensive representation of CSoS resilience degradation as standby losses escalate. With the mission-criticality factor set to $\eta = 0.65$ for defining $Q_{min}(t)$, system failure occurs at t =747 when losing 6 units, at t =810 with 4 units, and at t =853 with only 2 units lost. This confirms that standby unit redundancy directly strengthens the CSoS's resistance to disruptions, aligning with theoretical understandings of resilience enhancement via resource redundancy.

4.3.2. Resource replenishment strategy based on CSoS resilience

The proposed dual-dimension resilience assessment framework simultaneously elucidates both mission-oriented operational capabilities and inherent reserve potential, providing precise decision support for resource replenishment and mission adjustment during dynamic confrontations. Supplementing and replacing units are practical measures for enhancing CSoS robustness and resilience. However, the prioritization of resource supplementation remains a critical practical issue, which this research addresses through dual-dimension resilience analysis tailored to different resource supplementation types.

Based on the experiments described in Section 4.1, we compare changes in CSoS resilience between scenarios with and without resource supplementation. Additionally, we further analyze the differentiated impacts on CSoS resilience resulting

from supplementing reconnaissance units versus strike units. In our confrontation experiments, the primary mission objective is to attack and eliminate enemy units. Accordingly, the CSoS predominantly comprises strike units supported by a limited number of reconnaissance units.

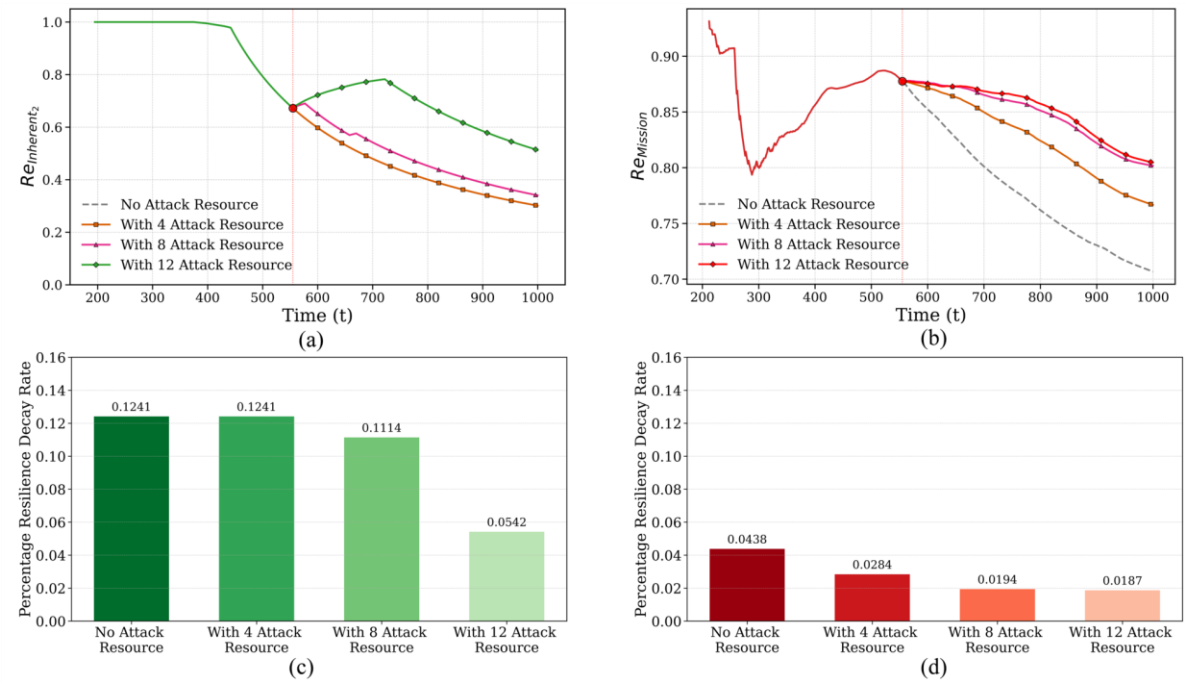

Figure 10. Comparison of resilience before and after supplementing strike units.

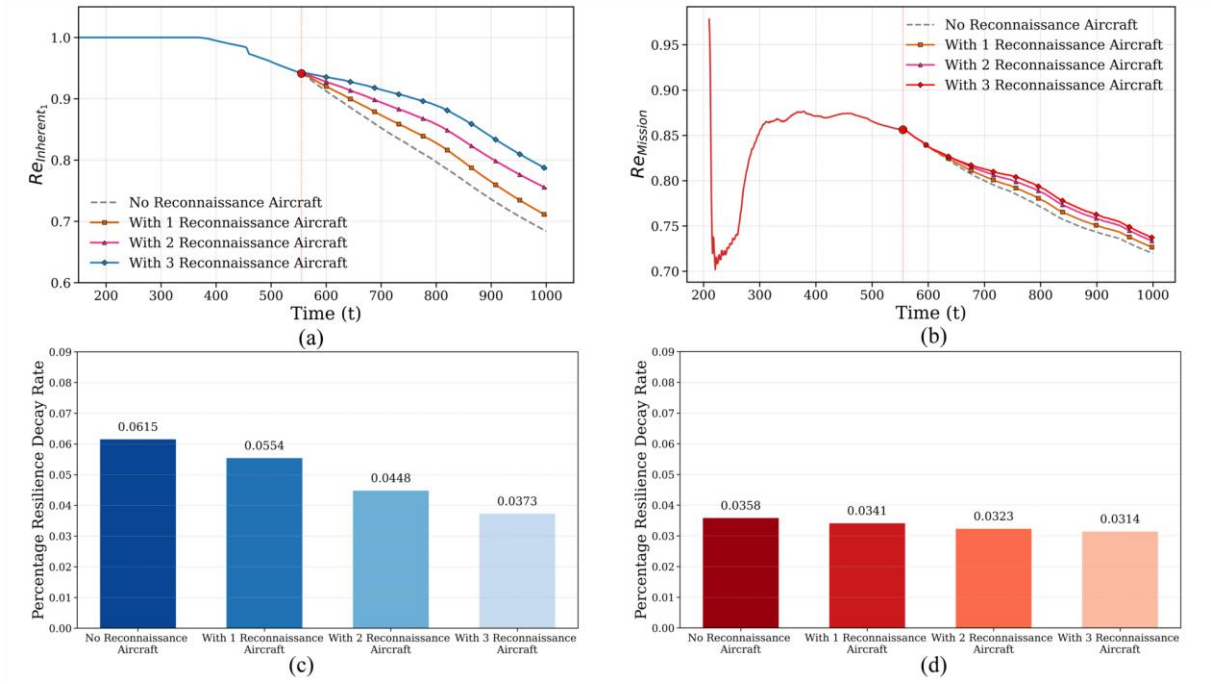

Figure 11. Comparison of resilience before and after supplementing with different quantities of reconnaissance units.

Fig. 10 illustrates the impact of supplementing with varying quantities of attack units at t =555. The line graphs in Fig. 10(a) and Fig. 10(b) demonstrate that increasing the number of supplementary attack resources leads to a more robust resilience profile for both inherent capability ($Re_{inherent}$) and mission capability ($Re_{misssion}$), mitigating the performance decline post-disruption.

To quantitatively assess these effects, the corresponding Percentage Resilience Decay Rates are presented in the bar charts in Fig. 10(c) and Fig. 10(d). Specifically, Fig. 10(c) shows the decay rate for inherent resilience; supplementing with

4 and 8 units shows a decay rate (0.1241 and 0.1114, respectively) comparable to the baseline, while a substantial supplement of 12 units significantly reduces the decay rate by over 56% to 0.0542. Fig. 10(d) shows that the decay rate of mission capability resilience has a more consistent dose-dependent response. The rate progressively decreases from 0.0438 (no resources) to 0.0187 (with 12 resources), a reduction of approximately 57%. This demonstrates that supplementing attack units simultaneously enhances operational effectiveness and strengthens strike reserve capacity, with both effects intensifying as the number of supplementary units increases.

Fig. 11 shows the resilience outcomes of supplementing reconnaissance-only units. As the number of supplementary aircraft increases from one to three, the degradation of $Re_{mission}$ is progressively slowed, while the effect on $Re_{inherent}$ remains minimal.

The Percentage Resilience Decay Rate (Fig. 11 (c), Fig. 11 (d)) confirms this trend. The decay rate of inherent resilience decreases from 0.0615 (no supplement) to 0.0373 (three aircraft), a reduction of nearly 40%, indicating that additional sensors help preserve the CSoS's latent "Observe" capability. By contrast, the decay rate of $Re_{mission}$ changes only slightly from 0.0358 to 0.0314, underscoring the limited value of redundant reconnaissance assets when mission perception is already sufficient. These results demonstrate that effective resource replenishment requires aligning supplementation with actual capability gaps while jointly considering both resilience dimensions to enable flexible strategies.

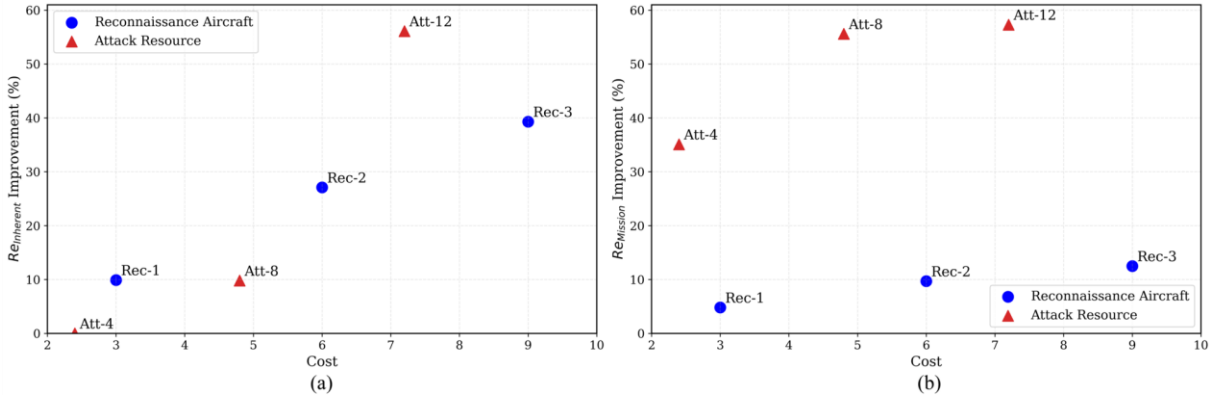

Figure 12. Cost-benefit analysis of supplementing reconnaissance vs. attack resources.

To further examine the redundancy–resource trade-offs, we extend the analysis with a cost–benefit perspective (Fig. 12). Relative cost values are assigned according to typical equipment differences (attack unit = 0.6, reconnaissance aircraft = 3). Fig. 12 (a) shows the relationship between cost and the improvement in $Re_{inherent}$, while Fig. 12 (b) shows the relationship for $Re_{mission}$. The results reveal two important insights. First, resilience gains exhibit diminishing marginal returns as resource quantities increase, particularly for $Re_{mission}$ (e.g., 12 attack units yield only a modest improvement compared to 8). Second, in this mission context, attack units provide a substantially higher benefit–cost ratio than reconnaissance aircraft. Specifically, the optimal strategy depends on the resilience dimension prioritized: maximizing ($Re_{inherent}$) favors supplementing 12 attack units (benefit–cost ratio= 7.79), whereas maximizing $Re_{mission}$ favors supplementing 4 attack units (benefit–cost ratio = 14.63).

In summary, our experimental results confirm that the proposed dual-dimension resilience evaluation model, by simultaneously quantifying the dynamic operational capabilities and inherent potential of standby units, effectively captures the latent recovery potential inherent within the CSoS. Unlike traditional single-dimensional approaches that tend to overestimate resilience by neglecting standby contributions, this approach facilitates accurate identification of critical replenishment timings and optimal resource supplementation strategies, thus preventing unnecessary resource expenditures and marginal benefit scenarios.

5. Application case: dynamic resilience of CSoS

5.1. Long-term confrontation scenario and data foundation

We employed simulation data from a representative multi-domain joint operational wargame scenario to validate the practical applicability of the proposed dynamic resilience model. The simulation involved an adversarial confrontation between

red and blue forces in a maritime operational area, as illustrated in Fig. 13. Both red and blue CSoS consisted of heterogeneous units operating across air, sea, land, and underwater domains (see Table 4). Throughout the scenario, adaptive mission scheduling enabled dynamic execution of offensive and defensive operations.

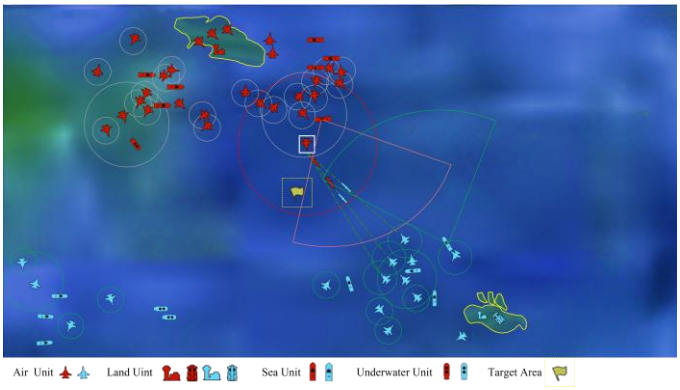

Figure 13. Wargame simulation scenario of the red-blue side confrontation process.

During the deployment phase, both sides conducted initial mission planning. Upon confrontation commencement, multi-domain unit sensors established comprehensive situational awareness. Based on the OODA loop, units dynamically adjusted mission assignments, executed closed-loop "reconnaissance–decision–strike" operations, and maintained continuous combat effectiveness via standby units. The simulation platform recorded detailed time-series datasets across 38 dimensions, including sensor data, unit status, mission actions, and simulation outcomes.

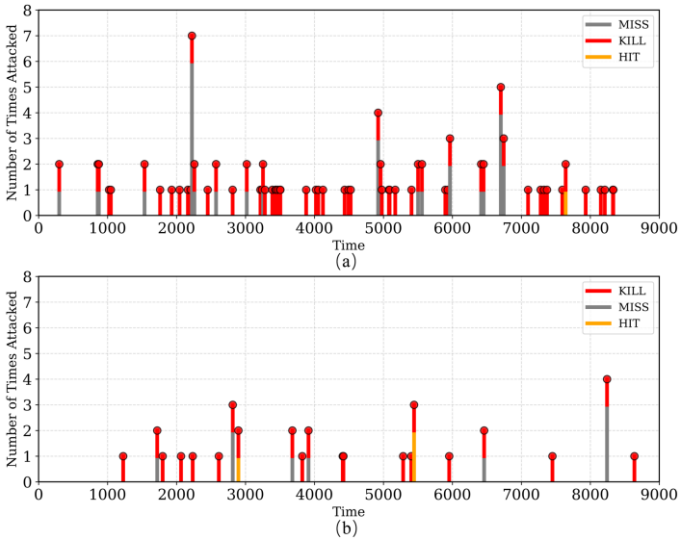

Figure 14. Spatiotemporal distribution of disruption events for red and blue sides.

Fig. 14 illustrates the temporal distribution of attack events, with panel (a) representing the distribution for the red side and panel (b) for the blue side. The cumulative effects of these events are shown up to each unit's final destruction event.

Table 4. Unit configurations for red and blue sides in the wargame simulation.

Time of Attack	Red Side (Quantity)	Blue Side (Quantity)
Air	81	78
Sea	13	8
Underwater	2	2
Land	9	9

Table 5. Identified resilience assessment phases for the red side.

Phase No.	Attacked units
1	U_A^{68}
2	$U_A^{65}, U_A^{67}, U_A^{70}, U_A^{87}$
3	$U_A^{35}, U_A^{36}, U_A^{45}, U_A^{47}, U_A^{50}, U_A^{51}, U_A^{57}, U_A^{59}, U_A^{62}, U_A^{66}, U_A^{69}, U_A^{71}, U_A^{75}, U_A^{79}, U_A^{80}, U_A^{83}, U_A^{84}, U_A^{93}, U_A^{95}, U_A^{97}, U_A^{102}, U_A^{103}$
4	$U_A^{39}, U_A^{43}, U_A^{46}, U_A^{60}, U_A^{72}, U_A^{76}, U_A^{101}$
5	$U_A^{29}, U_A^{31}, U_A^{33}, U_A^{41}, U_A^{48}, U_A^{49}, U_A^{52}, U_A^{55}, U_A^{61}, U_A^{86}, U_A^{96}, U_A^{109}$
6	$U_A^{32}, U_A^{34}, U_A^{37}, U_A^{38}, U_A^{54}, U_A^{56}, U_A^{77}, U_A^{78}, U_A^{81}, U_A^{85}, U_A^{90}, U_A^{94}, U_A^{}$

5.2. Multi-phase dynamic resilience analysis

We applied the dynamic phase-segmented resilience evaluation model (DPS-RE) from Section 3.2 to process disruption events in the simulated confrontation. As shown in Fig. 14, red side attacks exhibit significant spatiotemporal clustering (average interval: 131.7 time units), while blue side events show discrete distribution (average: 353 time units). Using the phase-merging strategy in equations (19)-(21), red side disruptions consolidated into 6 resilience evolution phases, and blue side into 11. Table 5 and Table 6 detail physical unit loss statistics for each side, respectively.

5.2.1. Dynamic resilience evolution analysis of both sides

Fig. 15 and Fig. 16 illustrate the resilience evolution of mission capability ($Re_{mission}$) and inherent capability ($Re_{inherent}$) for the red and blue sides.

First, mission capability resilience ($Re_{mission}$) demonstrates fluctuations closely associated with losses of mission-active units, accurately reflecting the immediate impacts of disruption events on combat effectiveness. However, relying solely on mission-active units can lead to an overestimation of resilience in later confrontation phases. For example, during Phase 6 of the red side, $Re_{mission}$ remained above 0.82 despite the loss of over 43.8% of total units (46 out of 105), clearly indicating a

significant disparity between measured resilience and actual combat capability degradation. Although mission capability resilience effectively characterizes instantaneous operational effectiveness, it insufficiently represents the overall resilience of the CSoS.

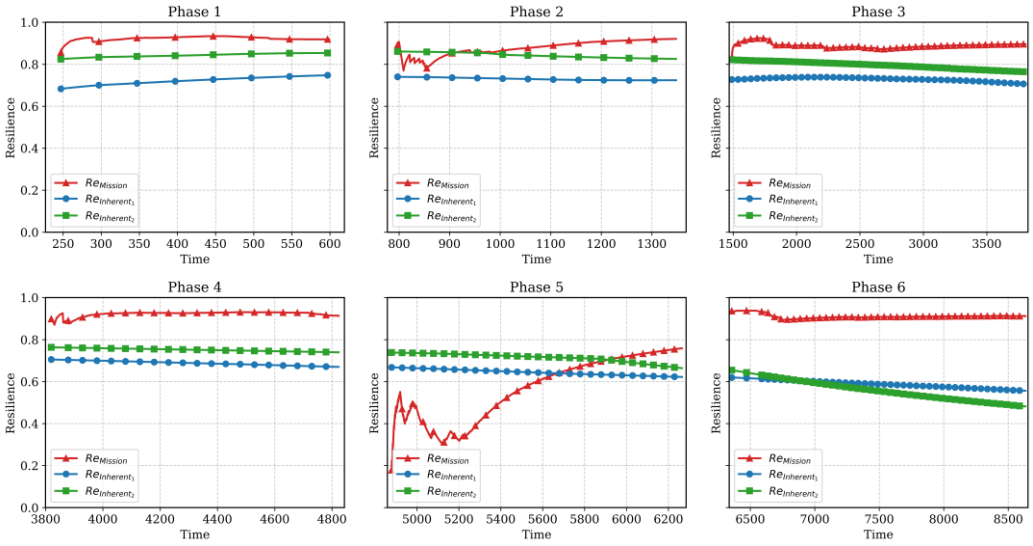

Figure 15. Multi-phase dynamic resilience trends for the red side.

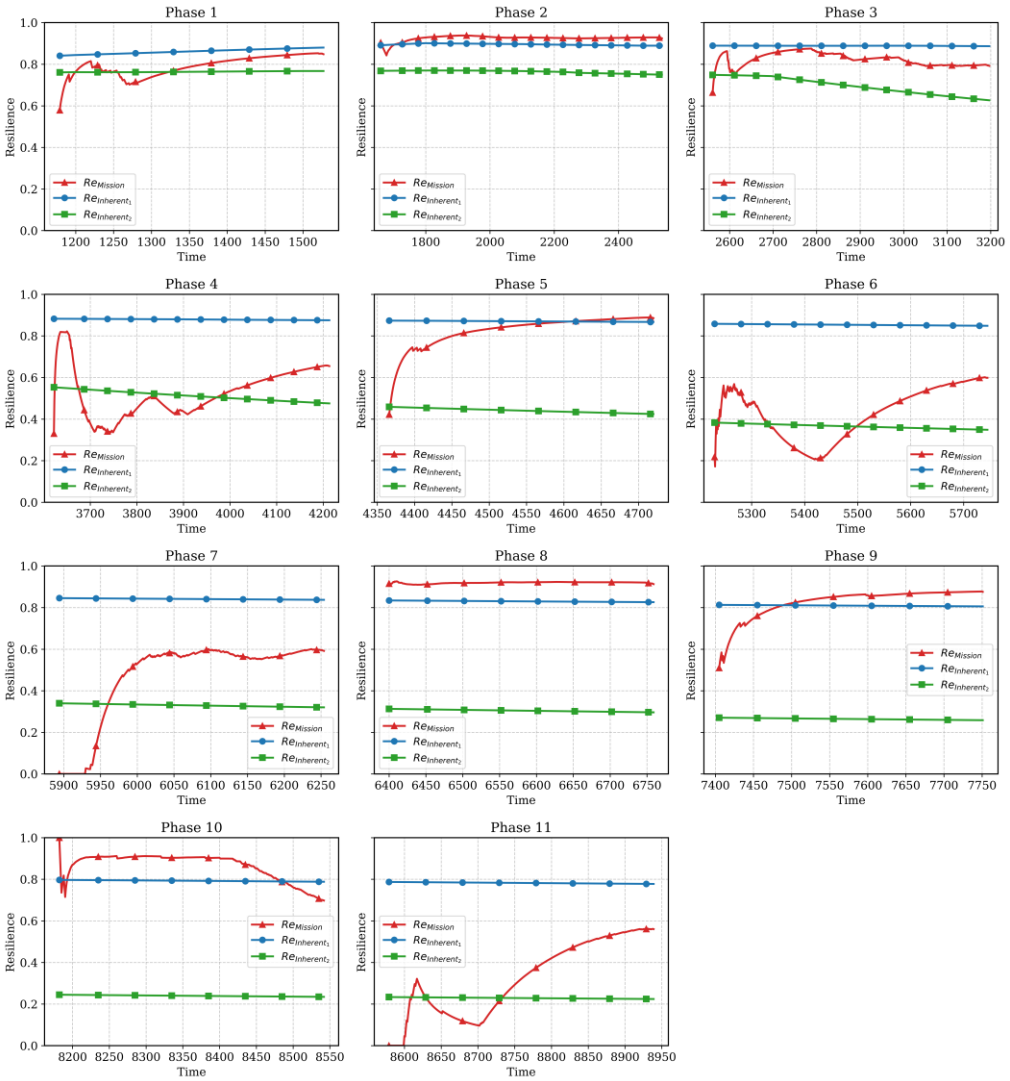

Figure 16. Multi-phase dynamic resilience trends for the blue side.

Table 6. Identified resilience assessment phases for the blue side.

Phase No.	Attacked units	Phase No.	Attacked units
1	U_A^{116}	7	U_A^{154}
2	$U_A^{141}, U_A^{159}, U_A^{166}, U_L^{15}$	8	U_A^{160}
3	$U_A^{121}, U_S^{156}, U_S^{18}$	9	U_A^{129}
4	$U_A^{122}, U_A^{139}, U_A^{151}$	10	U_A^{123}
5	U_A^{128}, U_A^{130}	11	U_A^{135}
6	$U_A^{170}, U_S^{14}, U_S^{20}$	-	-

Second, inherent capability resilience ($Re_{inherent}$) comprehensively quantifies changes in the overall available capabilities of the CSoS through two distinct indices. The reconnaissance perception index ($Re_{inherent1}$) explicitly reflects capability deterioration caused by unit losses, while the potential strike capability index ($Re_{inherent2}$) highlights weapon resource consumption trends. Notably, the red side's reconnaissance perception capability declined by 27.1%, substantially exceeding the blue side's 13.6%, consistent with the final simulation outcome (blue-side victory). These findings confirm that inherent capability resilience provides a robust indicator of sustained combat effectiveness over extended confrontation periods.

Overall, the proposed dual-dimensional resilience model integrating $Re_{mission}$ and $Re_{inherent}$ effectively captures critical resilience states of the CSoS. Specifically, when inherent resilience falls below an empirical threshold (e.g., 0.6), the CSoS transitions into a state of sustained capability degradation—even if mission capability resilience remains relatively high (> 0.7). Thus, this integrated approach provides decision-makers with precise insights into both immediate performance fluctuations and longer-term capability degradation trends, supporting informed decision-making for resource replenishment and mission adjustments in dynamic confrontation scenarios.

5.2.2. Comparative analysis of DPS-RE and traditional resilience evaluation methods

To highlight the advantages of the proposed DPS-RE model, we compared its evaluation results with those derived using a conventional Continuous Time-Resilience Evaluation (CT-RE) method, as illustrated in Fig. 17. Results indicate that the DPS-RE model demonstrates greater sensitivity in detecting resilience fluctuations, particularly in later confrontation stages. In contrast, the CT-RE method, which calculates resilience continuously across the entire confrontation period, tends to smooth resilience values over time, thus diminishing sensitivity due to cumulative effects. Although CT-RE effectively captures resilience disruptions in the early stages, it fails to distinctly reflect subsequent fluctuations. As shown in Fig. 17, DPS-RE (red line) clearly identifies resilience fluctuations, while CT-RE (grey line) remains relatively smooth

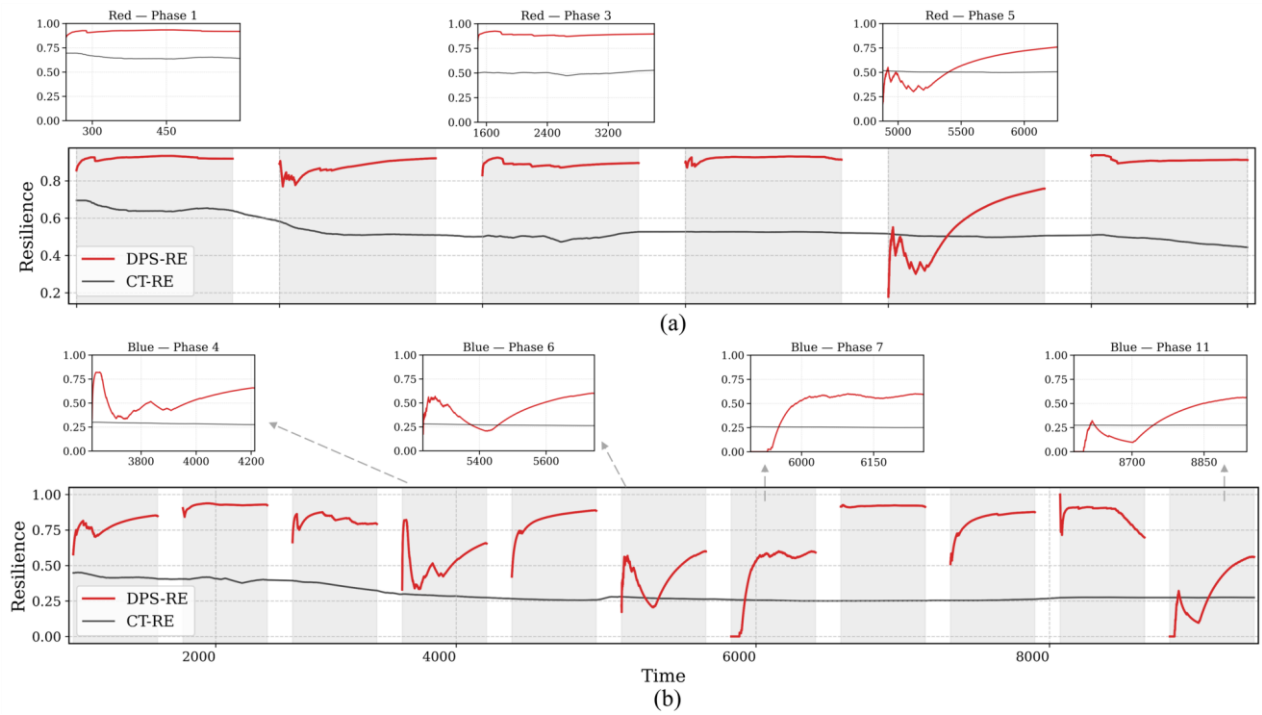

Figure 17. DPS-RE vs. CT-RE resilience evaluation (a) red side, (b) blue side.

Further comparative analysis was conducted using an Event Detection Density (EDD) indicator, defined as $EDD = N_{peak}/T_{phase}$, where N_{peak} denotes the number of peaks/troughs detected within a resilience phase, and T_{phase} represents phase duration. Table 7 and Table 8 demonstrate that the DPS-RE method achieved EDD values exceeding 0.5 events/min in approximately 82.4% of phases across both red and blue sides. In contrast, the CT-RE method failed to detect fluctuations ($EDD = 0$) in 69.2% of the assessed phases. These results clearly indicate that DPS-RE significantly outperformed CT-RE in capturing resilience fluctuations associated with disruption events, confirming its superior sensitivity and accuracy.

This case study verifies the potential application value of the dynamic resilience model in CSoS gaming. On one hand, through real-time fluctuation analysis of $Re_{mission}$, such as the rapid deterioration of mission capability in Red's Phase 5, vulnerable time windows of the CSoS can be quickly identified. On the other hand, it can be used for resource supply early warning. With $Re_{inherent} < 0.6$ set in this case, combined with the deterioration characteristics of the potential strike index and reconnaissance coverage, supply requirement windows can be precisely located, such as prioritizing strike unit replenishment for the red side at time point 6935 and the blue side at 3340.

Table 7. Comparison of multi-phase EDD indicators for the red side.

Phase No.	EDD	
	CT-RE	DPS-RE
1	0.1704	0.5114
2	0	0.8711
3	0.0259	0.0518
4	0	0.2393
5	0	0.6926
6	0	0.0263

Table 8. Comparison of multi-phase EDD indicators for the blue side.

Phase No.	EDD	
	CT-RE	DPS-RE
1	0	0.6896
2	0	0.6667
3	0	0.3334
4	0.1371	0.0686
5	0	0.4717
6	0	0.8122
7	0	0.6779
8	0	2.4466
9	0	0.6667
10	0	0
11	0	1.3873

6. Conclusion and future work

In this study, we proposed a dynamic resilience evaluation method for combat system of systems (CSoS) in long-term adversarial scenarios, integrating mission capability and inherent capability into a comprehensive assessment framework. To address unevenly distributed disruption events in prolonged confrontations, we developed a dynamic phase-segmented resilience evaluation model (DPS-RE) with time-varying performance baselines and expectation thresholds, enhancing evaluation sensitivity. Simulation experiments and multi-domain joint combat scenario analyses validated the method's effectiveness and applicability.

The main conclusions are as follows:

(1) Unlike traditional methods focused solely on mission-active units, the proposed dual-dimensional framework incorporates standby units' inherent capabilities, including reconnaissance perception and strike potential indices. This enables simultaneous assessment of instantaneous mission performance and latent recovery capacity, providing refined support for mission adjustments and resource replenishment in dynamic confrontations.

(2) The DPS-RE model mitigates sensitivity degradation from cumulative disruptions over extended periods. Experimental analyses showed significantly higher sensitivity and accuracy compared to traditional continuous methods, enabling rapid identification of vulnerability windows and precise timing for resource supplementation.

(3) Simulations varying standby unit numbers and types revealed a strong positive correlation between redundancy and CSoS resilience. Resource replenishment tailored to capability shortfalls reduced resilience deterioration rates by up to 57%. These findings provide valuable insights and quantitative references for optimizing CSoS robustness in real-world adversarial conditions.

Dynamic resilience assessment of CSoS under adversarial conditions remains a critical and challenging research domain within intelligent command and decision-making. This study provided a methodological framework and simulation-based validation for dynamic resilience assessment considering

mission-active and standby units. Nevertheless, future research can expand upon several aspects: (1) The dynamic interplay among heterogeneous units, particularly within communication interconnections and mission-specific kill chains, should be modeled to capture disruption propagation and inform the design of more robust operational architectures. (2) The current linear weighted summation may oversimplify complex coupling effects between capability dimensions. Future research should explore advanced integration methods, including nonlinear models or machine learning-based approaches, to better capture resilience dynamics under diverse scenarios. (3) Further investigation is needed into how different adversarial strategies drive resilience evolution. Systematic collection and analysis of rich confrontation data will clarify how combat tactics shape resilience outcomes and enable the design of adaptive resilience enhancement strategies.

References

1. Townsend S J. Accelerating multi-domain operations. Military Review 2018: 4–7.
2. Clark B, Patt D, Schramm H. Mosaic warfare: exploiting artificial intelligence and autonomous systems to implement decision-centric operations. Washington, DC, Center for Strategic and Budgetary Assessments: 2020.
3. Chen J, Sun J, Wang G. From unmanned systems to autonomous intelligent systems. Engineering 2022; 12: 1216–1219, https://doi.org/10.1016/j.eng.2021.10.007.
4. Li Z, Zhao D, Jiang J, Yang K, Chen Y. Capability oriented equipment contribution analysis in temporal combat networks. IEEE Transactions on Systems, Man, and Cybernetics: Systems 2021; 51(2): 696–704, https://doi.org/10.1109/TSMC.2018.2882782.
5. Zhi R, Zhang D, Tang S, Xiong W, Yang SH. Cooperative maneuver decision making for multi-UAV air combat based on incomplete information dynamic game. Defence Technology 2023; 27: 308–317, https://doi.org/10.1016/j.dt.2022.10.008.
6. Liu C, Sun S, Tao C, Shou Y, Xu B. Sliding mode control of multi-agent system with application to UAV air combat. Computers and Electrical Engineering 2021; 96: 107491, https://doi.org/10.1016/j.compeleceng.2021.107491.
7. Payuna U, Karen M. Exploiting stand-in redundancy to improve resilience in a system-of-systems (SoS). Procedia Computer Science 2013; 16: 532–541, https://doi.org/10.1016/j.procs.2013.01.056.
8. Paulette A, Cihan D. Modeling resilience in system of systems architecture. Procedia Computer Science 2016; 95: 111–118, https://doi.org/10.1016/j.procs.2016.09.300.
9. Dreesbeimdiek K M, von Behr C M, Brayne C, Clarkson P J. Towards a contemporary design framework for systems-of-systems resilience. Proceedings of the Design Society 2022; 2: 1835–1844, https://doi.org/10.1017/pds.2022.186.
10. Holling C S. Resilience and stability of ecological systems. Annual Review of Ecology and Systematics 1973; 4: 1–23, https://doi.org/10.1146/annurev.es.04.110173.000245.
11. Dakos V, Kéfi S. Ecological resilience: what to measure and how. Environmental Research Letters 2022; 17(4): 043003, https://doi.org/10.1088/1748-9326/ac5767.
12. Yi C, Jackson N. A review of measuring ecosystem resilience to disturbance. Environmental Research Letters 2021; 16(5): 053008, https://doi.org/10.1088/1748-9326/abdf09.
13. Gülçin B, Öykü I, Orhan F. A review of urban resilience literature. Sustainable Cities and Society 2022; 77: 103579, https://doi.org/10.1016/j.scs.2021.103579.
14. Datola G. Implementing urban resilience in urban planning: a comprehensive framework for urban resilience evaluation. Sustainable Cities and Society 2023; 98: 104821, https://doi.org/10.1016/j.scs.2023.104821.
15. Rojas J F, Patil P, Masterson A M, Bradley T H, Ekti A R, Asher Z D. Automated vehicle lane centering system requirements informed by resilience engineering and a solution using infrastructure-based sensors. IEEE Access 2024; 12: 97605–97620, https://doi.org/10.1109/ACCESS.2024.3422266.
16. Barrero-Arciniegas H, Asghar A A, Davide D, Erwin R, Dominik T M. Design parameters for resilience in cyber-physical production systems. Procedia Computer Science 2025; 253: 2316–2326, https://doi.org/10.1016/j.procs.2025.01.292.
17. Liu J, Xu R, Li J, Yang K, Lou Z. Enhancing the resilience of combat system-of-systems under continuous attacks: novel index and reinforcement learning-based protection optimization. Expert Systems with Applications 2024; 251: 123912, https://doi.org/10.1016/j.eswa.2024.123912.

18. Wang Y, Tao J, Zhang X, Bai G, Zhang Y. Mission-oriented capability evaluation for combat network based on operation loops. Defence Technology 2024; 42: 156–175, https://doi.org/10.1016/j.dt.2024.07.002.
19. Sun Q, Li H, Wang Y, Zhang Y. Multi-swarm-based cooperative reconfiguration model for resilient unmanned weapon system-of-systems. Reliability Engineering and System Safety 2022; 222: 108426, https://doi.org/10.1016/j.ress.2022.108426.
20. Jiao T, Li X, Wang J, Luo A. Resilience evaluation method of combat system-of-systems based on hierarchical structure. In: 2024 5th International Conference on Computer Engineering and Application (ICCEA); 2024: 1503–1508, https://doi.org/10.1109/ICCEA62105.2024.10603630.
21. Chen Z, Hong D, Cui W, Xue W, Wang Y, Zhong J. Resilience evaluation and optimal design for weapon system of systems with dynamic reconfiguration. Reliability Engineering and System Safety 2023; 237: 109409, https://doi.org/10.1016/j.ress.2023.109409.
22. Han Q, Pang B, Li S, Li N, Guo P, Fan C, Li W. Evaluation method and optimization strategies of resilience for air & space defense system of systems based on kill network theory and improved self-information quantity. Defence Technology 2023; 21: 219–239, https://doi.org/10.1016/j.dt.2023.01.005.
23. Liu T, Bai G, Tao J, Zhang Y, Fang Y, Xu B. Modeling and evaluation method for resilience analysis of multi-state networks. Reliability Engineering and System Safety 2022; 226: 108663, https://doi.org/10.1016/j.ress.2022.108663.
24. Liu T, Bai G, Tao J, Zhang Y, Fang Y. A multistate network approach for resilience analysis of UAV swarm considering information exchange capacity. Reliability Engineering and System Safety 2024; 241: 109606, https://doi.org/10.1016/j.ress.2023.109606.
25. Zhu Y, Bai G, Xu Z, Wang L, Xu B. Disintegrating the information exchange network of UAV swarm based on relative resilience. Reliability Engineering and System Safety 2026; 266: 111745, https://doi.org/10.1016/j.ress.2025.111745.
26. Zhang C, Liu T, Bai G, Tao J, Zhu W. A dynamic resilience evaluation method for cross-domain swarms in confrontation. Reliability Engineering and System Safety 2024; 244: 109904, https://doi.org/10.1016/j.ress.2023.109904.
27. Kong L, Wang L, Cao Z, Wang X. Resilience evaluation of UAV swarm considering resource supplementation. Reliability Engineering and System Safety 2024; 241: 109673, https://doi.org/10.1016/j.ress.2023.109673.
28. Zhao X, Wang C, Wang S, Han H. Standby component replacement strategy for a balanced system with a standby pool. Reliability Engineering and System Safety 2025; 254: 110627, https://doi.org/10.1016/j.ress.2024.110627.
29. Wang X, Gao X, Wang L, Su X, Jin J, Liu X, Deng Z. Resilient multi-objective mission planning for UAV formation: a unified framework integrating task pre- and re-assignment. Defence Technology 2025; 45: 203–226, https://doi.org/10.1016/j.dt.2024.08.002.
30. Wang N, Wu M, Yuen K F. Modelling and assessing long-term urban transportation system resilience based on system dynamics. Sustainable Cities and Society 2024; 109: 105548, https://doi.org/10.1016/j.scs.2024.105548.
31. Tian T, Liang Y, Peng Z, Cheng Y, Chen K. Assessing the dynamic resilience of urban rail transit networks during their evolution using a ridership-weighted network. PLOS ONE 2023; 18(9): e0291639, https://doi.org/10.1371/journal.pone.0291639.
32. Bai G, Li Y, Fang Y, Zhang Y, Tao J. Network approach for resilience evaluation of a UAV swarm by considering communication limits. Reliability Engineering and System Safety 2020; 193: 106602, https://doi.org/10.1016/j.ress.2019.106602.
33. Henry D, Ramirez-Marquez J E. Generic metrics and quantitative approaches for system resilience as a function of time. Reliability Engineering and System Safety 2012; 99: 114–122, https://doi.org/10.1016/j.ress.2011.09.002.
34. Uday P, Marais K B. Resilience-based system importance measures for system-of-systems. Procedia Computer Science 2014; 28: 257–264, https://doi.org/10.1016/j.procs.2014.03.033.
35. Uday P, Marais K. Designing resilient systems-of-systems: a survey of metrics, methods, and challenges. Systems Engineering 2015; 18(5): 491–510, https://doi.org/10.1002/sys.21325.
36. Watson B C, Chowdhry A, Weissburg M J, Bras B. A new resilience metric to compare system of systems architecture. IEEE Systems Journal 2022; 16(2): 2056–2067, https://doi.org/10.1109/JSYST.2021.3062444.
37. Watson BC, Morris Z B, Weissburg M, Bras B. System of system design-for-resilience heuristics derived from forestry case study variants. Reliability Engineering and System Safety 2023; 229: 108807, https://doi.org/10.1016/j.ress.2022.108807.
38. Chen W, Li W, Zhang T. Complex network-based resilience capability assessment for a combat system of systems. Systems 2024; 12(1): 31, https://doi.org/10.3390/systems12010031.
39. Zhang X, Mahadevan S, Sankararaman S, Goebel K. Resilience-based network design under uncertainty. Reliability Engineering and

System Safety 2018; 169: 364–379, https://doi.org/10.1016/j.ress.2017.09.009.

40. Fan JR, Li DG, Li RP, Wang Y. Analysis on MAV/UAV cooperative combat based on complex network. Defence Technology 2020; 16(1): 150–157, https://doi.org/10.1016/j.dt.2019.09.002.
41. Xu R, Liu J, Li J, Yang K, Zio E. Tsosra: a task-oriented resilience assessment framework for system-of-systems. Reliability Engineering and System Safety 2024; 248: 110186, https://doi.org/10.1016/j.ress.2024.110186.
42. Chen Z, Zhao T, Jiao J, Chu J. Performance-threshold-based resilience analysis of system of systems by considering dynamic reconfiguration. Proceedings of the Institution of Mechanical Engineers, Part B: Journal of Engineering Manufacture 2022; 236(14): 1828–1838, https://doi.org/10.1177/0954405420937528.
43. Tran H T, Balchanos M, Domercant J C, Mavris D N. A framework for the quantitative assessment of performance-based system resilience. Reliability Engineering and System Safety 2017; 158: 73–84, https://doi.org/10.1016/j.ress.2016.10.014.
44. Zhong Y, Li H, Sun Q, Huang Z, Zhang Y. A kill chain optimization method for improving the resilience of unmanned combat system-of-systems. Chaos, Solitons and Fractals 2024; 181: 114685, https://doi.org/10.1016/j.chaos.2024.114685.
45. Feng Q, Liu M, Dui H, Cai B, Fan D, Ren Y, Wang Z. A general design-oriented resilience measurement and evaluation method for engineering systems: resilience cube. Reliability Engineering and System Safety 2024; 245: 110038, https://doi.org/10.1016/j.ress.2024.110038.
46. Sun Y, Li Y, Li H, Liu J, Zhou X. Intuitionistic fuzzy MADM in wargame leveraging with deep reinforcement learning. IEEE Transactions on Fuzzy Systems 2024; 32(9): 5033–5045, https://doi.org/10.1109/TFUZZ.2024.3435400.
47. Mittal V, Davidson A. Combining wargaming with modeling and simulation to project future military technology requirements. IEEE Transactions on Engineering Management 2021; 68(4): 1195–1207, https://doi.org/10.1109/TEM.2020.3017459.
48. Yang D, Li Q, Zhu F, Cui H, Yi W, Qin J. Parallel emergency management of incidents by integrating OODA and PREA loops: the C2 mechanism and modes. IEEE Transactions on Systems, Man, and Cybernetics: Systems 2023; 53(4): 2160–2172, https://doi.org/10.1109/TSMC.2022.3229036.
49. Yadav P, Kim S. OODA loop for learning open-world novelty problems. Advances in Computers 2024; 134: 91–130, https://doi.org/10.1016/bs.adcom.2023.06.002.
50. Pan X, Wang H, Yang Y, Zhang G. Resilience based importance measure analysis for SoS. Journal of Systems Engineering and Electronics 2019; 30(5): 920–930, https://doi.org/10.21629/JSEE.2019.05.10.
51. Hu T, Zong Y, Lu N, Jiang B. Toward the resilience of UAV swarms with percolation theory under attacks. Reliability Engineering and System Safety 2025; 254: 110608, https://doi.org/10.1016/j.ress.2024.110608.

List of Notations

i, j	Indices for unit i and enemy unit j.	$R_i^{(m)}$	Combat radius of unit i in domain m.
θ_i, θ_j	Heading angles of unit i and j.	$P_i^{(m)}$	Engagement success probability of unit i.
$c_{\alpha_{ij}}$	Angle perception between i and j.	$A_i^{(m)}$	Strike potential of unit i.
v_i, v_j	Velocity perception between i and j.	ω_m	Weight for strike potential in domain m.
cv_{ij}	Velocity perception between unit i and j.	C_{act}	CSoS strike potential.
D_{ij}	Distance between unit i and j.	N_m	Number of units in domain m.
R_a, R_s	Attack and perception ranges.	α	Adaptive weight (reconnaissance vs. strike).
cd_{ij}	Distance perception between i and j.	λ	Sensitivity coefficient.
s_{ij}	Survival probability of unit i.	$Q_{inherent}$	Inherent capability of the CSoS.
SU_i	Survival rate of unit i.	Q_{min}	Minimum performance threshold.
N_0	Number of mission-active units.	η_j	Mission-criticality factor.
$Q_{mission}$	Mission capability of the CSoS.	Q_{opt}	Optimal performance level.
r_i	Detection radius of unit i.	$Q_{initial}^{(J)}$	Pre-disruption performance of dimension j.
$\mathcal{D}_i$	Sensor set of unit i.	β	Weight between time resilience and performance resilience.
d_k	Sensor k on unit i.	Re_0	Time resilience.
$r_{i,k}^{max}$	Maximum detection radius of sensor d_k.	Re_1	Performance resilience.
$e_{i,k}$	Activation state of sensor d_k.	$Re_{mission}$	Mission capability resilience.
δ_i	Sensor indicator for unit i.	Re_0'	Discretized time resilience.

N_u	Number of units with active perception.	Re_1'	Discretized performance resilience.
N	Total number of units in the CSoS.	$Re_{inherent}$	Inherent capability resilience.
C_{obs}	Reconnaissance perception index of CSoS.	$\mathcal{T}$	Multi-phase confrontation process.
m	Operational domain index.	E_k	k -th phase of the process.
$W_i^{(m)}$	Weapon resources of unit i in domain m.	Re_{SoS}	Final dynamic resilience of the CSoS.